PHYSICAL REVIEW B **81**, 241103(R) (2010)

Effects of anisotropic charge on transverse optical phonons in NiO: Inelastic x-ray scattering spectroscopy study

H. Uchiyama,[1,2] S. Tsutsui,[2] and A. Q. R. Baron[1,2]
[1]*Material Dynamics Laboratory, RIKEN, Sayo, Hyogo 679-5148, Japan*
[2]*Japan Synchrotron Radiation Research Institute, Koto, Sayo, Hyogo 679-5198, Japan*
(Received 6 May 2010; published 23 June 2010)

Phonon dispersion of detwinned NiO is measured using inelastic x-ray scattering. It is found that, near the zone center, the energy of the transverse-optical-phonon mode polarized parallel to the antiferromagnetic order is ~1 meV lower than that of the mode polarized perpendicular to the order, at room temperature. This is explained via anisotropic polarization of the Ni and O atoms, as confirmed using a Berry's phase approach with first-principles calculations. Our explanation avoids an apparent contradiction in previous discussions focusing on Heisenberg interaction.

DOI: 10.1103/PhysRevB.81.241103 PACS number(s): 75.50.Ee, 63.20.dd, 75.30.Gw, 77.84.Bw

Transition-metal mono-oxides are fundamental materials for studying properties of magnetic and strongly correlated systems. Among them, NiO and MnO are antiferromagnetic (AFM) insulators with similar crystal structure and physical properties. The AFM order and lattice contraction occur along the [111] direction below the Néel temperature (T_N =523 K for NiO). The order consists of ferromagnetic (111) planes. Above T_N, both have a rocksalt structure. NiO and MnO are relatively simple, because they have nondegenerate electronic ground states, and are free from Jahn-Teller effects, unlike FeO and CoO.[1]

The magnetism of these materials is often discussed in terms of a superexchange mechanism. MnO has antiferromagnetic interactions both in the nearest-neighbor (J_1) and next-nearest-neighbor (J_2) exchanges, and these interactions reproduce the experimental results.[2,3] On the other hand, J_1 for NiO still remains uncertain, perhaps because it is much smaller than the antiferromagnetic superexchange J_2 interaction, which is responsible for the AFM order. For example, local spin-density approximation (LSDA)+U calculations give ferromagnetic J_1 (Ref. 3) while some calculations such as GW show antiferromagnetic J_1.[4] Experimentally, a measurement of spin-wave dispersion indicates ferromagnetic J_1 (Ref. 5) while one of magnetic susceptibility suggests antiferromagnetic J_1.[6]

Another issue is that LSDA+U calculation results are not easily reconciled with the exchange-interaction picture of NiO. According to Refs. 2 and 7, the lattice distortion is dominated by J_1 with no contribution from J_2, and antiferromagnetic J_1 causes the contraction in [111], if $|J_1|$ decreases with increasing the distance between the nearest-neighbor Ni atoms. Based on this discussion, the calculated ferromagnetic J_1 (Ref. 3) is not consistent with the calculated[8] (and observed) contraction in NiO, suggesting an additional ingredient is needed to understand the calculation results.

The energy of transverse optical (TO) phonons can be used as a direct probe of microscopic coupling;[9] TO modes that would be degenerate in a cubic rocksalt structure, are split at the zone center under the AFM order, with the energy of the mode polarized along the order ($E_{\parallel}^{TO}$) different than that of the mode polarized in the plane perpendicular to the order ($E_{\perp}^{TO}$). As discussed in Ref. 3 the sign of this difference ($E_{\parallel}^{TO}-E_{\perp}^{TO}$) can be linked to the sign of J_1. The picture is generally consistent for MnO, where the observed shift[10,11] is in agreement with theory,[3,8] however question remains about NiO, where preliminary measurements[10] disagree with the LSDA+U calculations.[3,8]

We have made careful measurements of the TO-phonon dispersion in detwinned NiO at room temperature (RT), and find $E_{\parallel}^{TO}-E_{\perp}^{TO}\sim-1.0$ meV in the vicinity of the zone center, in reasonable agreement with the LSDA+U calculations.[3,8] In order to understand this, we introduce the anisotropic polarization derived from a Berry's phase.[12] This anisotropy yields an anisotropic effective Born charge, which was introduced into AFM materials by Ref. 9, after tremendous success in ferroelectric materials. This spin-dependent term dominates the splitting and provides the missing ingredient to explain the observed lattice distortion and phonon splitting simultaneously.

NiO samples with (111) surface were detwinned in accordance with Ref. 13, giving the AFM order and lattice contraction along the [111] direction (in this report, indices of cubic symmetry are used). The single structural domain (T domain) was confirmed by the (333) Bragg peak [Fig. 1(a)]; a peak from another domain with a different direction for the contraction, if any, would appear at lower angle [the bar in Fig. 1(a)]. NiO may also have different type of domains, originating from the different spin-axis orientation (S domain). However, Ref. 14 shows that a field of >2 kOe along $[1\bar{1}0]$ may be used to align the spin axes along $[11\bar{2}]$. When the field reaches 5 kOe, a single S domain is obtained,[14] but the T-domain wall starts to move.[13] Considering these facts, magnetic field of 4.5 kOe was applied parallel to $[1\bar{1}0]$ during the measurements.

Phonon measurements using inelastic x-ray scattering (IXS) were performed at BL35XU of SPring-8 (Ref. 15) with a total-energy resolution of ~1.6 meV and a momentum resolution of ~0.08 $Å^{-1}$. The incident energy is 21.75 keV. The measurements were achieved at RT [~300 K ($<T_N$)] to prevent introducing a new domain caused by tiny stresses or thermal gradients.[13,14] We also performed similar measurements under 1.7 kOe at some phonon vectors to study field-induced effects, such as magnetoelectric effects. The results show the same phonon peak positions as at 4.5

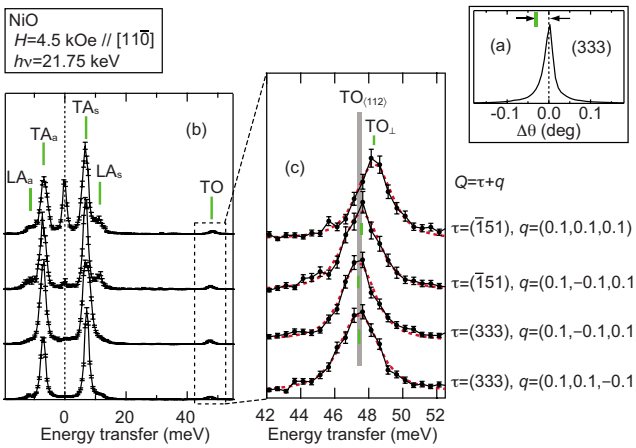

FIG. 1. (Color online) (a) The θ scan around the (333) Bragg peak. The bar indicates the expected peak position of $\{33\bar{3}\}$. (b) IXS spectra at $|q|=(0.1,0.1,0.1)$. LA denotes longitudinal-acoustic phonon. TA_s (LA_s) indicates the Stokes line of TA (LA) while TA_a (LA_a) does the anti-Stokes line. (c) The enlarged view of (b) at around the TO phonons. Dotted lines are results of curve fitting and the bars show the peak positions.

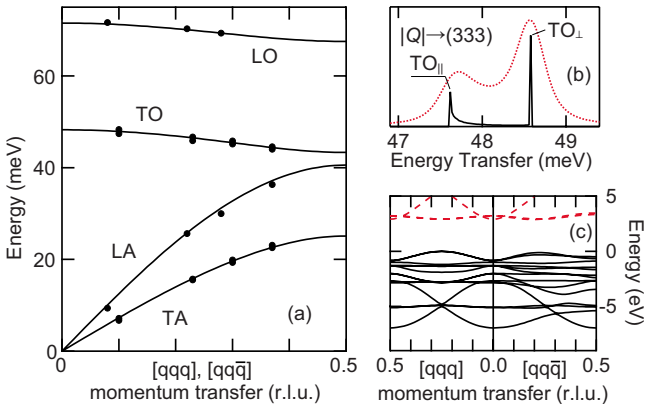

FIG. 2. (Color online) (a) Phonon dispersion of NiO in the $|q|=[qqq]$ direction, which is determined theoretically (lines), and experimentally (the dots). (b) Simulated TO-phonon distribution in the vicinity of $|Q|=(333)$ (solid line). Dotted line shows the spectrum broadened by a 0.4 meV resolution function. (c) The band structure along [qqq] and [qq$\bar{q}$] obtained by LSDA+U. Solid lines are the valence bands, which are used in calculating the Berry's phase of polarization.

kOe, within an experimental accuracy of ±0.3 meV. We confirmed the zero energy using the midpoint of the Stokes and anti-Stokes lines of the transverse-acoustic (TA) phonons.

Figures 1(b) and 1(c) shows the IXS spectra at a phonon vector of $|q|=(0.1,0.1,0.1)$, where $q=Q-\tau$; Q is the total momentum transfer, and τ is the nearest Bragg point. A shift is observed, depending on the choice of momentum transfer. For the top spectrum, where q is parallel to [111], the polarization vector of the observed transverse mode must be in the plane perpendicular to the [111] ordering direction. For the others, the situation is less well defined, and we will discuss it again in the context of specific models. However, naively, one would expect the polarization vectors to be within and perpendicular to the plane defined by the [111] axis and q. In this case, at the chosen total momentum vectors, Q, the mode polarized in the plane would tend to dominate the lower three spectra.

Simulations were carried out using shell-model calculations,[16] which describe phonon dispersion, with only a few parameters, very well especially for NiO and MnO.[17,18] The OPENPHONON source code[19] was used for the calculations, and most of the parameters were taken from Ref. 17.[20] The shell model has several types of parameters including the atomic position, Coulomb interaction (charge), including the core-shell interaction, and short-range Born-von Kármán force constants between pairs of atoms. As seen in Fig. 2(a), the calculations assuming the cubic structure reproduce the present experimental phonon dispersion very well. This agreement in dispersion lends credence to the idea that our approach, below, of modifying successively, the various components of the shell model, can be used to understand the material's behavior.

First, just the effect of the noncubic lattice was considered, holding all the other parameters fixed. The experimental lattice distortion of ~90.06° at RT (Ref. 13) gives TO-phonon splitting of ~0.06 meV at $|q|=(0.1,0.1,0.1)$. This value is much smaller than the observed in Fig. 1(c), suggesting that only the lattice distortion cannot describe the observed TO peak shift.

Next we introduce additional Born-von Kármán force constants to simulate the anisotropy of the Heisenberg exchange interaction. Effectively, the shell model includes J_2 in the longitudinal force constant between nearest-neighbor Ni-O atoms. As for J_1, additional force constants along $\langle 01\bar{1}\rangle$ (between parallel spin, T) and $\langle 011\rangle$ (between antiparallel spin, $-T$) were included [as the cubic structure assumed, J_1 deviation due to the lattice distortion[2] ($J_1^{\pm}$) is not considered]. The parameter T was varied to fit the experimental results.

Using these additional force constants, the polarization vectors for the peaks in Fig. 1(c) can be determined as eigenvectors of the dynamical matrix. The spectra at $q=(0.1,0.1,-0.1)$ and $(0.1,-0.1,0.1)$ with $\tau=(333)$ are assigned to the modes polarized close to [112] ($TO_{[112]}$) and [121] ($TO_{[121]}$), respectively. For $q=(0.1,-0.1,0.1)$ with $\tau=(\bar{1}51)$, the spectrum is dominated by the $TO_{[121]}$ mode, while the spectra at $q=(0.1,0.1,0.1)$ with $\tau=(\bar{1}51)$ is assigned to $TO_\perp$. In short, it is estimated from the experiment that the energy of $TO_{\langle 112\rangle}$ ($E^{TO}_{\langle 112\rangle}$) is ~0.9 meV lower than $E^{TO}_\perp$.

The intensity around the zone center is simulated using the parameters above. Figure 2(b) shows the calculated TO line shape (solid line) near $|Q|=(333)$ consists of two parts; a delta-functionlike $TO_\perp$ peak and distribution from $TO_\parallel$ to $TO_\perp$ resulting from the direction dependence of $q\to 0$. From Fig. 2(b), difference between $E^{TO}_\parallel$ and $E^{TO}_\perp$ is estimated as ~1.0 meV. The value at RT agrees reasonably with the results of the LSDA+U calculations ($E^{TO}_\parallel - E^{TO}_\perp = -1.8$ meV),[3,8] which generally assume $T=0$. Furthermore, when this spectrum is convolved with a 0.4 meV resolution function (dotted line), it is clearly seen that

$TO_\perp$ has stronger intensity than other components. The stronger $TO_\perp$ intensity agrees with the observation in MnO.[10,11]

Both the phonon splitting and lattice contraction for NiO are correctly predicted by the LSDA+U calculations. However, conceptually LSDA+U does not fit the superexchange mechanism well; the calculated ferromagnetic J_1 and lattice contraction require increasing $|J_1|$ with increasing r in the exchange framework (r indicates the distance between the nearest-neighbor Ni atoms), since the lattice distortion is proportional to $-\partial J_1/\partial r$.[2,7] Moreover, this contradicts the relation, suggested in Ref. 3, between the sign of $E_\parallel^{TO}-E_\perp^{TO}$ and that of J_1. Thus, some additional ingredient is required, which is included in the calculations but not in the exchange framework, in order to explain the experimental observation.

The last perturbation we consider is an anisotropic Coulomb interaction. The effective Born charge tensor, Z^*, was estimated using LSDA+U as implemented in the ABINIT package.[21] $U=4$ eV was chosen to fit the experimental valence band,[22,23] mainly because the calculations for the Berry's phase of polarization only require the occupied states [solid lines in Fig. 2(c)]. The calculated charge tensor of Ni is

$$Z_{Ni}^* = \begin{pmatrix} z^* & \Delta z^* & \Delta z^* \\ \Delta z^* & z^* & \Delta z^* \\ \Delta z^* & \Delta z^* & z^* \end{pmatrix}, \quad (1)$$

where $z^*=2.26$ and $\Delta z^*=0.03$. For oxygen (Z_O^*), $z^*=-2.26$ and $\Delta z^*=-0.03$ are obtained independently, satisfying the charge neutrality. This gives an anisotropic parameter, $\Delta z^*/z^*=1.3\times10^{-2}$. The principal directions and values of the tensor show that each atom has an anisotropic charge of $z^*+2\Delta z^*$ parallel to the AFM order, [111], ($Z_\parallel^*$) and $z^*-\Delta z^*$ perpendicular to [111] ($Z_\perp^*$). The anisotropy results from the asymmetric band dispersion; the AFM order brings about band folding in the [qqq] direction [Fig. 2(c)], while no folding occurs in the $\langle qq\bar{q}\rangle$ directions, leading to the effective charge anisotropy. Hence this charge anisotropy is spin dependent, extending, somewhat, the limits of Anderson's original discussion.[24]

This anisotropic change may be introduced into the shell model in different ways. In particular, the detailed formulation of the shell model introduces matrices for the total charges Z, shell charges Y, and core-shell force constants k. We could introduce anisotropy into any of these, Z, Y, k, and here we consider explicitly Z and Y.

The free-ion polarizability is given by Y^2e^2/k so that we first consider introducing the anisotropy in Y. Assuming the off-diagonal components, $Y_{ij}(i\neq j)$, for both O and Ni have a common value of $Y_{ij}/Y_{ii}=2.8\times10^{-2}$, we can reproduce the experimental results in Fig. 1(c) and all assignments mentioned above. Based on Ref. 16, which discusses the shell model in detail for a rocksalt structure, we then estimate the effective charge anisotropy as $\Delta z^*/z^*=5.6\times10^{-2}$ ($z^*=\pm2.21$).

Alternatively, we consider introductions of anisotropy directly in the static charge, Z, of the shell model. Taking $Z_{ij}/Z_{ii}=3\times10^{-3}$ is sufficient to reproduce the results. This

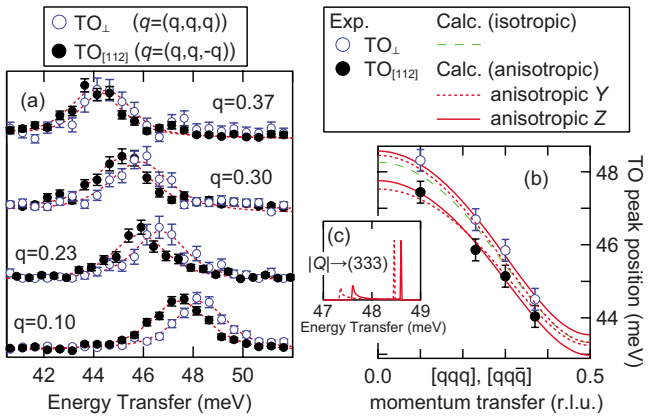

FIG. 3. (Color online) (a) TO-phonon dispersion in the [111] and [11$\bar{1}$] directions. Dotted lines are results of curve fitting. (b) Comparison of $TO_\perp$ and $TO_{[112]}$ phonon modes between experimental (marks) and theoretical (lines) results. The calculations are based on the shell model with (solid and dotted lines)/without (dashed lines) effective charge anisotropy. (c) Simulated TO-phonon distribution for the effective charge anisotropy in the vicinity of $|Q|=(333)$.

value corresponds to $\Delta z^*/z^*=8\times10^{-3}$ ($z^*=\pm2.19$). This agrees better with the LSDA+U calculations than the value from the anisotropic Y case above. However, it is also possible the larger $\Delta z^*/z^*$ value is caused by lack of consideration of higher-order moments than dipole in the shell model.[16]

It is interesting to consider if this anisotropy might be related to the static contraction along the [111] direction. According to Ref. 25, Born effective charges have a correlation to the covalent bonding. This suggests the lattice distortion can be explained using the anisotropic Born charge, as a distance between two atoms at equilibrium may depend on the magnitude of the charges. Noting that the principle directions of Z^* are orthogonal, the lattice distortion from cubic to rhombohedral can be estimated using Ref. 26. In the anisotropic Z case, $\Delta z^*/z^*=8\times10^{-3}$ gives the lattice distortion of 90.15°, in fair agreement with the measured 90.06° at room temperature.[13] If we take $\Delta z^*/z^*=5.6\times10^{-2}$, the distortion in the case of anisotropic Y is estimated, giving a large value, 91.11°.

The measured momentum dependence of the splitting is in agreement with both of these (anisotropic Y or anisotropic Z) models as can be seen in Figs. 3(a) and 3(b). One notes that in all models, the phonon splitting is reduced toward the zone boundary, and the magnitude at the zone boundary depends on the detailed model. However, our resolution does not allow us to choose between the models. Meanwhile, Fig. 3(c) depicts the TO distribution near $|Q|=(333)$ for anisotropic Y and Z, showing the similar distribution to Fig. 2(b) for the anisotropic force constant. It should be noted that, based on Ref. 16, it is confirmed that these anisotropic charge models satisfy the generalized Lyddane-Sachs-Teller relation[27,28] both along and perpendicular to the [111] direction.

In conclusion, we have two different methods of including the anisotropy of the material that fit our experimental results

for the phonon splitting: (1) *ad hoc* addition of force constants to mimic a possible Heisenberg interaction and (2) inclusion of an anisotropy in the electrostatic terms of the shell model. The latter, which, qualitatively seems to match the anisotropy of the Born effective charge tensor calculated using the LSDA+U method, seems a more reasonable choice. Furthermore, the latter description provides an additional ingredient that allows one to reconcile the observed lattice contraction with the ferromagnetic J_1 interactions calculated using LSDA+U.[3,8]

These discussions suggest the anisotropic polarization should be considered in studying AFM compounds. Both the Berry's phase calculations of polarization and Heisenberg exchange interaction have spin-dependent anisotropy. However, the exchange interaction applies to only magnetic atoms, while the anisotropic effective charge applies to both magnetic and nonmagnetic atoms, as required by charge neutrality. In addition, in order to estimate the exchange interaction precisely, a deviation of the Wannier functions from the cubic symmetry should be considered, even if the lattice is assumed as cubic. This may be relevant to other AFM materials, for example, high-T_c cuprates or iron pnictides.

In summary, we observed TO-phonon shifts for detwinned NiO at room temperature, and found that the energy of the TO phonon with atomic motions in the direction of the [111] magnetic ordering is ~1.0 meV lower than the TO mode with motions perpendicular to the ordering direction, near the zone center. We suggest this observation is most simply explained by considering the anisotropic polarization of the medium. While ultimately related to a spin-dependent interaction, at a conceptual level this is an additional ingredient that should be considered, to understand the material behavior, distinct from the exchange interaction.

The synchrotron radiation experiments were performed at the BL35XU in the SPring-8 with the approval of the Japan Synchrotron Radiation Research Institute (Proposal No. 2008A1584).

[1] J. Kanamori, Prog. Theor. Phys. **17**, 197 (1957).
[2] M. E. Lines and E. D Jones, Phys. Rev. **139**, A1313 (1965); **141**, 525 (1966).
[3] W. Luo, P. Zhang, and M. L. Cohen, Solid State Commun. **142**, 504 (2007).
[4] T. Kotani and M. van Schilfgaarde, J. Phys.: Condens. Matter **20**, 295214 (2008).
[5] M. T. Hutchings and E. J. Samuelsen, Phys. Rev. B **6**, 3447 (1972).
[6] R. Shanker and R. A. Singh, Phys. Rev. B **7**, 5000 (1973).
[7] T. Yamada, J. Phys. Soc. Jpn. **18**, 520 (1963).
[8] S. Y. Park and H. J. Choi, Phys. Rev. B **80**, 155122 (2009).
[9] S. Massidda, M. Posternak, A. Baldereschi, and R. Resta, Phys. Rev. Lett. **82**, 430 (1999).
[10] E. M. L. Chung, D. McK. Paul, G. Balakrishnan, M. R. Lees, A. Ivanov, and M. Yethiraj, Phy. Rev. B **68**, 140406(R) (2003).
[11] T. Rudolf, Ch. Kant, F. Mayr, and A. Loidl, Phys. Rev. B **77**, 024421 (2008).
[12] R. Resta and D. Vanderbilt, in *Physics of Ferroelectrics*, edited by C. H. Ahn, K. M. Rabe, and J. M. Triscone (Springer-Verlag, Berlin, 2007), p. 31.
[13] G. A. Slack, J. Appl. Phys. **31**, 1571 (1960).
[14] H. Kondoh and T. Takeda, J. Phys. Soc. Jpn. **19**, 2041 (1964); E. Uchida, N. Fukuoka, H. Kondoh, T. Takeda, Y. Nakazumi, and T. Nagamiya, *ibid.* **23**, 1197 (1967).
[15] A. Q. R. Baron, Y. Tanaka, S. Goto, K. Takeshita, T. Matsushita, and T. Ishikawa, J. Phys. Chem. Solids **61**, 461 (2000).
[16] A. D. B. Woods, W. Cochran, and B. N. Brockhouse, Phys. Rev. **119**, 980 (1960); R. A. Cowley, W. Cochran, B. N. Brockhouse, and A. D. B. Woods, *ibid.* **131**, 1030 (1963).
[17] W. Reichardt, V. Wagner, and W. Kress, J. Phys. C **8**, 3955 (1975).
[18] V. Wagner, W. Reichardt, and W. Kress, Proceedings of the Conference on Neutron Scattering, 1976 (unpublished), Vol. 1, p. 175.
[19] A. Mirone and M. d'Astuto, available at http://sourceforge.net/projects/openphonon
[20] Slight modification of some parameters is achieved to suit the experimental results better; $B'_{12}=-5.07$ and $B_{22}=0.13$ (e^2/v) are different from Ref. 17.
[21] X. Gonze, J.-M. Beuken, R. Caracas, F. Detraux, M. Fuchs, G.-M. Rignanese, L. Sindic, M. Verstraete, G. Zerah, F. Jollet, M. Torrent, A. Roy, M. Mikami, Ph. Ghosez, J.-Y. Raty, and D. C. Allan, Comput. Mater. Sci. **25**, 478 (2002); M. Torrent, F. Jollet, F. Bottin, G. Zerah, and X. Gonze, *ibid.* **42**, 337 (2008).
[22] Q. Yin, A. Gordienko, X. Wan, and S. Y. Savrasov, Phys. Rev. Lett. **100**, 066406 (2008).
[23] Z.-X. Shen, R. S. List, D. S. Dessau, B. O. Wells, O. Jepsen, A. J. Arko, R. Barttlet, C. K. Shih, F. Parmigiani, J. C. Huang, and P. A. P. Lindberg, Phys. Rev. B **44**, 3604 (1991).
[24] P. W. Anderson, Phys. Rev. **115**, 2 (1959).
[25] M. Posternak, R. Resta, and A. Baldereschi, Phys. Rev. B **50**, 8911 (1994).
[26] I. D. Brown and D. Altermatt, Acta Crystallogr., Sect. B: Struct. Sci. **41**, 244 (1985).
[27] W. Cochran and R. A. Cowley, J. Phys. Chem. Solids **23**, 447 (1962).
[28] R. M. Pick, M. H. Cohen, and R. M. Martin, Phys. Rev. B **1**, 910 (1970).